ISSN 0036-0244, Russian Journal of Physical Chemistry A, 2019, Vol. 93, No. 10, pp. 1957–1964. © Pleiades Publishing, Ltd., 2019.
Russian Text © The Author(s), 2019, published in Zhurnal Fizicheskoi Khimii, 2019, Vol. 93, No. 10, pp. 1556–1563.

ON THE 90th ANNIVERSARY OF THE DEPARTMENT OF CHEMISTRY OF THE MOSCOW STATE UNIVERSITY

Effect of Cobalt on the Catalytic Properties of Platinum during the Oxidation of CO: Experimental Data and Quantum-Chemical Simulation

D. A. Pichugina[a,*], N. A. Nikitina[a], N. E. Kuz'menko[a], and D. I. Potemkin[b,c]

[a] *Department of Chemistry, Moscow State University, Moscow, 119991 Russia*

[b] *Boreskov Institute of Catalysis, Russian Academy of Sciences, Novosibirsk, 630090 Russia*

[c] *Novosibirsk State University, Novosibirsk, 630090 Russia*

**e-mail: daria@phys.chem.msu.ru*

Received March 15, 2019; revised March 15, 2019; accepted April 9, 2019

Abstract—The oxidation of CO over Pt and Pt–Co catalysts was studied both experimentally and by quantum-chemistry calculations. Density functional theory simulation shows that CO is oxidized on Pt_{13} via dissociative oxygen adsorption. The calculated activation energy for the dissociation of O_2 on Pt_{13} is 56 kJ/mol. It is found that when a cobalt atom is introduced into the cluster, the activation energy falls for the stages of CO oxidation and the dissociation of O_2. Catalytic tests performed on Pt and $Pt_{0.5}Co_{0.5}$ nanopowders confirm the Pt–Co system displays high activity in the oxidation of CO.

Keywords: CO oxidation, reaction mechanism, catalysis, nanocluster, bimetallic particle

DOI: 10.1134/S0036024419100212

INTRODUCTION

Quantum-chemical simulation is a modern research tool for predicting the properties of transition metals in catalytic reactions of practical importance [1, 2]. For example, the new composition of a Co–Mo bimetallic catalyst in the synthesis of ammonia was predicted with the density functional theory [3]. The main advantage of quantum-chemical simulations of catalytic processes is the ability to study reaction mechanisms, including transition metal nanoparticles incorporated into promising heterogeneous catalysts, while avoiding the use of expensive experimental equipment.

Developing low-temperature catalysts for the oxidation of CO is an important problem. Platinum and its various forms (nanoparticles, atomic clusters, and isolated atoms stabilized on the surfaces of oxide carriers), is normally used in this process [4–7]. For the oxidation of CO on platinum, the Langmuir–Hinshelwood, Mars–Van Krevelen, and Eley–Rideal mechanisms were proposed [8]. The Langmuir–Hinshelwood mechanism includes the stages of CO and O_2 adsorption (molecular or dissociative) on the active center of a catalyst:

$$CO \xrightarrow{Pt} CO, \quad (1)$$

$$O_2 \xrightarrow{Pt} O_2^*, \quad (2a)$$

$$O_2 \xrightarrow{Pt} 2O^*. \quad (2b)$$

CO_2 is formed through carbonate or peroxide intermediates:

$$CO^* + O_2^* \xrightarrow{Pt} OOCO^* \xrightarrow{Pt} CO_2 + O^*, \quad (3)$$

$$CO^* + 2O^* \xrightarrow{Pt} OC(O)O^* \xrightarrow{Pt} CO_2 + O^*. \quad (4)$$

The mechanism of CO oxidation on platinum is determined by many factors, e.g., the size and shape of a particle and the type of carrier [9]. One of the most promising ways of affecting the catalytic activity of platinum is to incorporate another metal into the composition of the catalyst, e.g., iron, nickel, cobalt, or copper [10–14]. It was found in [15] that Pt–M nanoparticles with ordered structure improve a material's catalytic properties. Special centers with certain compositions of metal atoms (the geometric effect) and a charge created by the redistribution of electron density between two metals (electronic effect) form inside a bimetallic catalyst [14, 16].

In this work, we studied the mechanism of CO oxidation on Pt_{13} and $Pt_{12}Co$ by quantum chemical means. We also simulated the structure of clusters, their interaction with O_2 and CO, and their oxidation.

The theoretical data are compared to experimental results on the catalytic properties of Pt and $Pt_{0.5}Co_{0.5}$ nanopowders.

EXPERIMENTAL

The structure of Pt_{13} and $Pt_{12}Co$ clusters and their complexes with O_2 and CO was optimized and their energies calculated using the PBE (Perdew–Burke–Ernzerhof) density functional theory [17] in combination with the SBKJC basis set and pseudopotentials [18]. The contribution from zero-point energies was determined from their oscillation frequencies, calculated in the harmonic approximation. The structure of transition states (TSes) was localized, and the activation energies (E_a) in the stages of CO oxidation were calculated with the Bernie optimization algorithm [19]. TSes were found using the IRC algorithm, which includes studying the relationship between the energy of a reaction system and a reaction coordinate [20]. The calculations were performed with the PRIRODA program [21] on the *Lomonosov* supercomputer at Moscow State University [22].

The oxidation of CO was studied on Pt and $Pt_{0.5}Co_{0.5}$ nanopowders (disordered solid solution) obtained by decomposing $[Pt(NH_3)_4](NO_3)_2 \cdot 2H_2O$ and $[Pt(NH_3)_4][Co(C_2O_4)_2(H_2O)_2] \cdot 2H_2O$, respectively [23]. The nanopowders were chosen as samples due to the ease of controlling their structure and the absence of carrier influence.

The obtained single-phase Pt and $Pt_{0.5}Co_{0.5}$ nanopowders were described thoroughly in [23, 24]. The surface areas of the samples were additionally measured via the chemisorption of CO (10 ± 2 m^2/g).

The catalytic properties in the oxidation reaction of CO were studied in a U-shaped quartz flow reactor (inner diameter, 3 mm) at atmospheric pressure. The mass of the catalyst in the reactor was 25 mg (fraction, ≤0.1 mm) [25]. The temperature was measured with a chromel-alumel (K-type) thermocouple placed into the center of the catalyst layer.

Our catalytic experiments were performed in a mixture with 1.0 vol % CO and 1.0 vol % O_2, using He as a balance. The feed rate of the reaction mixture was 80000 $cm^3\ g^{-1}\ h^{-1}$. The composition and concentrations of the components of the gas phase upstream and downstream of the reactor were determined on a KHROMOS GKH-1000 chromatograph. Before each experiment, the nanopowders were reduced for 1 h in H_2 at 200°C. The catalysts were then kept for 15 min in a reaction mixture at 25°C, and the catalytic properties were determined in several cycles of temperature rise and fall. The catalytic characteristics of Pt were stable for at least 20 h in several temperature cycles. There was slow reversible deactivation on $Pt_{0.5}Co_{0.5}$ as a result of repeated reduction, due probably to the segregation of cobalt oxide on its surface. A detailed study of this phenomenon is beyond the scope of this work. The properties of $Pt_{0.5}Co_{0.5}$ obtained in the first cycle of temperature rise and fall were used for purposes of comparison.

The oxidation of CO was characterized from the conversion of CO (X_{CO}), calculated according to the equation

$$X_{CO} = \frac{[CO]_{input} - [CO]_{output}}{[CO]_{input}} \times 100\%, \quad (5)$$

where $[CO]_{input}$ and $[CO]_{output}$ are the concentrations of CO at the input and output, respectively.

RESULTS AND DISCUSSION

Quantum-Chemical Study of the Structure and Catalytic Properties of Pt_{13} and $Pt_{12}Co$ Clusters during the Oxidation of CO

The structure of a Pt_{13} cluster was calculated at the first stage. The results from calculating the structure of this cluster by quantum-chemical means are contradictory [27–32], even though it was obtained experimentally [26]. Six Pt_{13} isomers in the triplet electronic state were considered. The optimized structures of the clusters and their energies relative to that of the most stable isomer **1** are shown in Fig. 1. Isomer **1** is a distorted pyramid, in the base of which are eight platinum atoms. A similar structure was predicted for Pt_{13} in [31, 32]. It should be noted that isomers **2–4** differ negligibly in their energies (no more than 18 kJ/mol), compared to isomer **1**, indicating possible isomerization of the cluster. It is known that such structurally non-rigid properties of particles result in both the activation of reagents and their subsequent transformation during catalytic processes [33, 34].

The structure and energy of bimetallic $Pt_{12}Co$ clusters with different arrangements of Co atoms were calculated (Fig. 1). The most energy stable cluster was $Pt_{12}Co\_2$, in which cobalt is on the edge. It should be noted that the initial structure of a monometallic cluster remains unchanged, but the multiplicity of $Pt_{12}Co$ grows to eight, as was observed in [35]. Introducing cobalt into a platinum cluster increases the multiplicity and alters the magnetic properties of a particle.

The oxidation of CO on Pt_{13} and $Pt_{12}Co\_2$ (referred to below as $Pt_{12}Co$) was simulated. Superoxide $Pt_{13}O_2$ and peroxide $Pt_{12}OOPt$ complexes appear when Pt_{13} interacts with O_2 (Fig. 2). The calculated changes in energy during the interaction between clusters and oxygen (Table 1) indicate that the formation of $Pt_{12}OOPt$ cluster, in which vertex and edge platinum atoms participate in the bridge coordination of

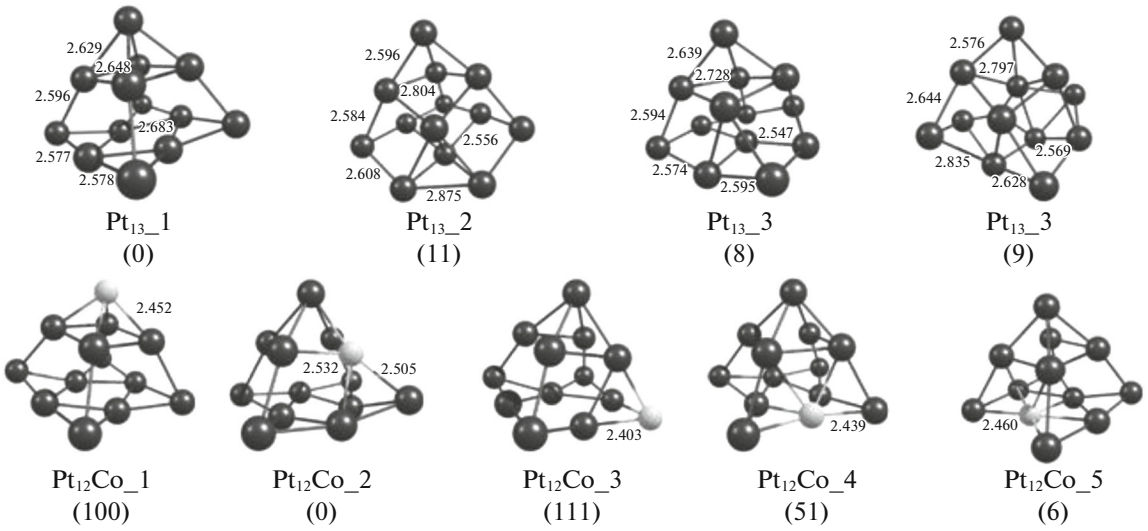

Fig. 1. Optimized structures of Pt_{13} and $Pt_{12}Co$ clusters. The relative energies of isomers are given in parentheses (in kJ/mol). A cobalt atom is shown in light grey.

O_2, is the one most advantageous. The transitional state of the destruction of the O–O bond in $Pt_{12}OOPt$ was identified. The calculated activation energy for the dissociation of O_2 on Pt_{13} was 56 kJ/mol.

When a $Pt_{12}Co$ cluster interacts with O_2, a $CoPt_{11}OOPt$ peroxide complex is formed in which oxygen coordinates on platinum atoms (Fig. 2). The dissociation of oxygen in $CoPt_{11}OOPt$ passes through a low activation barrier (29 kJ/mol) lower than the one in $Pt_{12}OOPt$.

A CO molecule interacts with Pt_{13} to form the stable $Pt_{13}CO$ complex. A $CoPt_{12}CO$ complex in which a CO molecule bonds to the platinum atom on the edge is the most advantageous of the 13 different ways of coordinating CO on $Pt_{12}Co$.

When O_2 and CO are activated on Pt_{13}, there is a co-adsorption effect. Adding CO to oxidized $Pt_{13}O_2$ and $Pt_{12}OOPt$ clusters is more energy efficient than adding it to Pt13, while adding O_2 to $Pt_{13}CO$ is more advantageous than adding it to Pt_{13} (Table 1). There was no co-adsorption effect of O_2 and CO on $Pt_{12}Co$. We may therefore assume that CO is coordinated on Pt_{13} with a low coordination number at the first stage, and O_2 then bonds at the edge–vertex center in peroxide form. The subsequent oxidation of CO was considered for two intermediates, $Pt_{13}O_2CO$ and $Pt_{12}(CO)OOPt$.

Figure 3 shows the energy diagram of the multistep oxidation of CO on Pt_{13}. The first stage of the formation of a IM_1 peroxide intermediate has the highest activation energy. As a result, the oxidation of CO on Pt_{13} is more likely to proceed through IM_1' or through a mechanism that includes the dissociation of O_2,

$$Pt_{13} + O_2 \rightarrow Pt_{12}OOPt + 126\ \text{kJ/mol},$$

$$Pt_{12}OOPt \rightarrow OPt_{13}O + 20\ \text{kJ/mol}\ (E_a = 56\ \text{kJ/mol}),$$

and oxidation of CO with the participation of O* (through intermediates IM_2', IM_3', IM_4'):

$$Pt_{13}O(\text{vertex}) + CO \rightarrow Pt_{13}OCO + 191\ \text{kJ/mol},$$

$$Pt_{13}OCO \rightarrow Pt_{13}{-}OCO + 34\ \text{kJ/mol}\ (E_a = 70\ \text{kJ/mol}),$$

$$Pt_{13}{-}OCO \rightarrow Pt_{13} + CO_2 - 33\ \text{kJ/mol}.$$

Table 1. Change in energy ΔE (kJ/mol) of the stages of CO oxidation on Pt_{13} and $Pt_{12}Co$

Stage	Pt_{13}	$Pt_{12}Co$
$M + O_2 \rightarrow MO_2$	–72	—
$M + O_2 \rightarrow M_{12}OOM$	–126	–156
$M_{12}OOM \rightarrow OM_{13}O$	–20	–34
	(56)	(29)
$M_{13} + CO \rightarrow M_{13}CO$	–154	–199
$M_{13}O_2 + CO \rightarrow M_{13}O_2CO$	–172	—
$M_{12}OOM + CO \rightarrow M_{12}OOMCO$	–152	–188
$M_{13}CO + O_2 \rightarrow M_{12}(CO)OOM$	–179	–149

Activation energies E_a are given in parentheses (in kJ/mol).

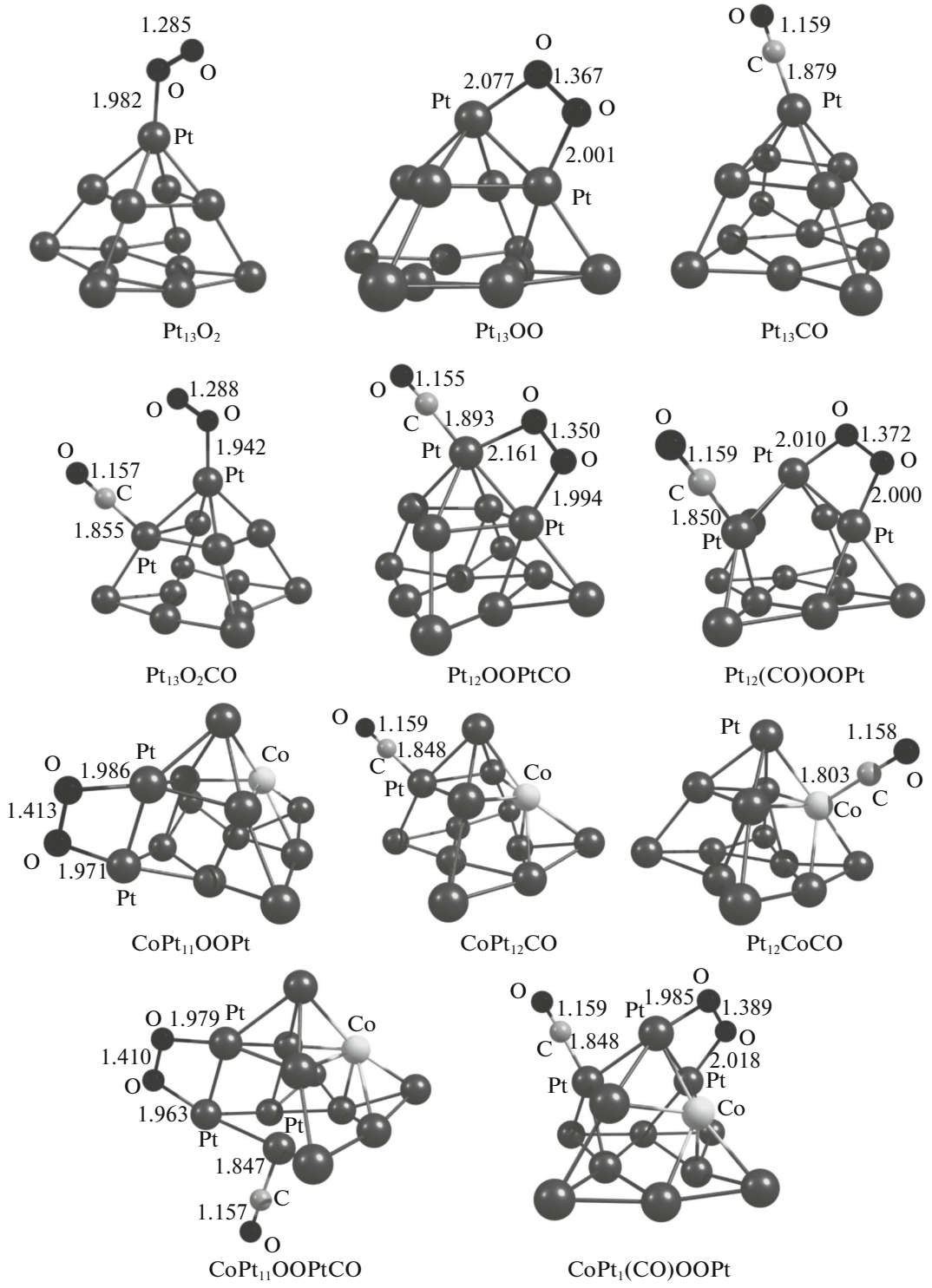

Fig. 2. Optimized structures of Pt_{13} and $Pt_{12}Co$ complexes with O_2 and CO.

Figure 4 shows the energy diagram of the oxidation of CO on $Pt_{12}Co$ for two intermediates, $CoPt_{11}(CO)OOPt$ and $CoPt_{11}OOPtCO$. In contrast to Pt_{13}, the process does not proceed through a carbonate intermediate but through the dissociation of O_2. The activation energy for the first stage of CO oxidation is reduced considerably, relative to that of Pt_{13}. The path of CO oxidation from $CoPt_{11}(CO)OOPt$ is more kinetically and thermodynamically advantageous than the one from

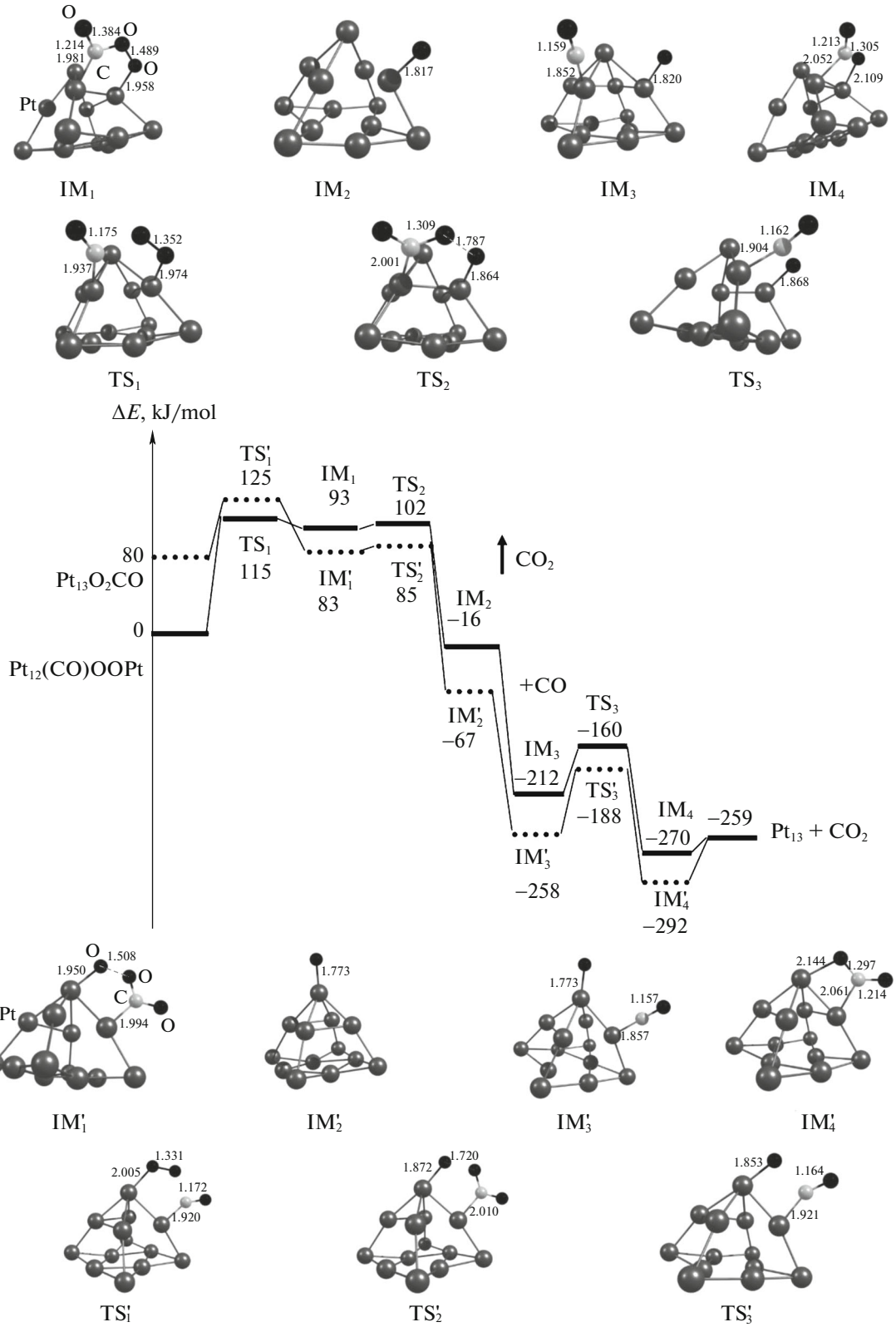

Fig. 3. Energy diagram of the oxidation of CO on Pt_{13}.

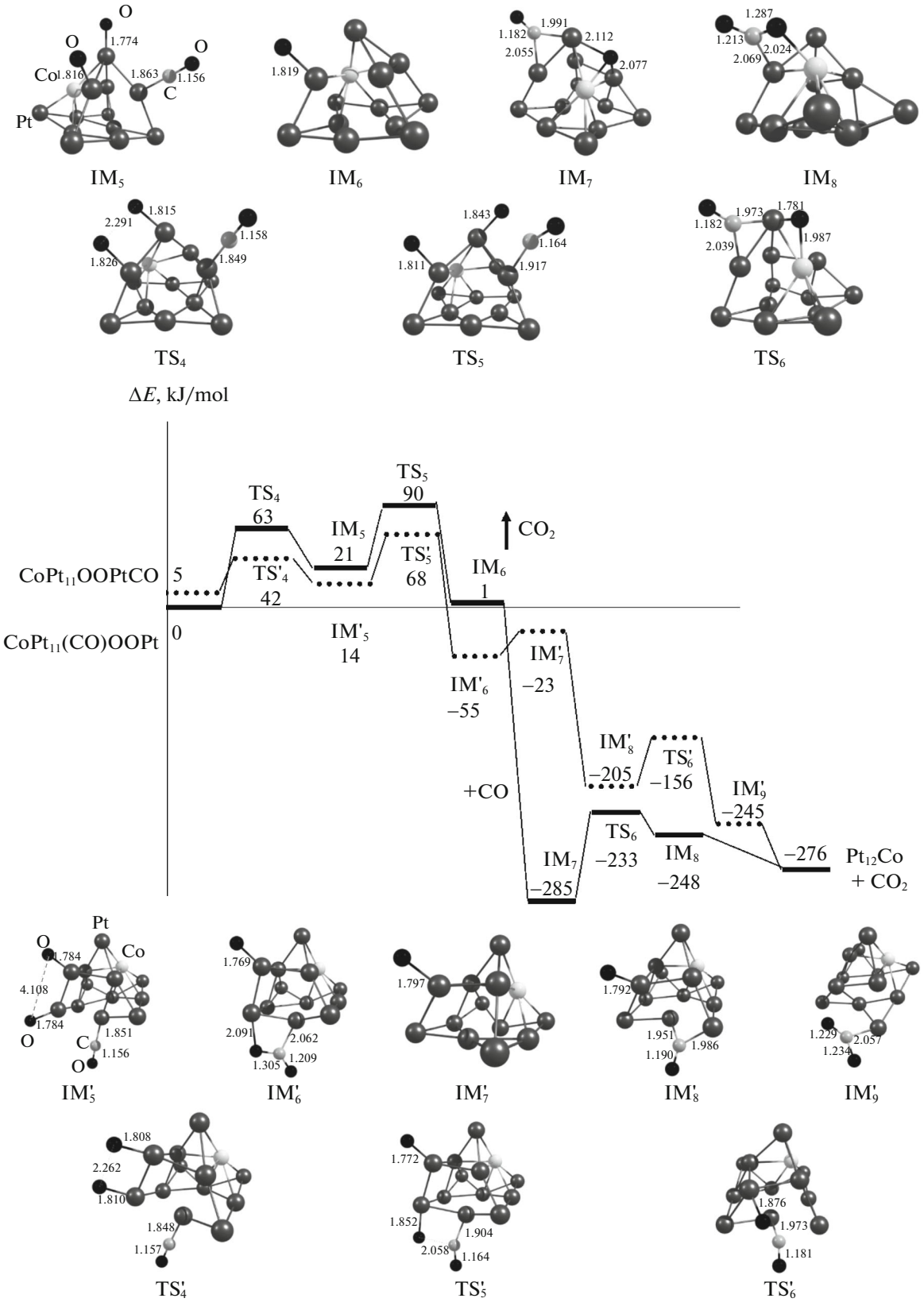

Fig. 4. Energy diagram of the oxidation of CO on $Pt_{12}Co$.

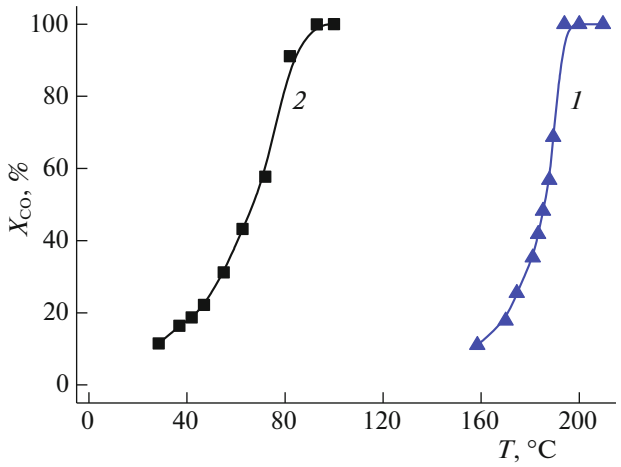

Fig. 5. (Color online) Temperature dependences of the conversion of CO during the complete oxidation of CO on (*1*) Pt and (*2*) $Pt_{0.5}Co_{0.5}$ nanopowders.

$CoPt_{11}OOPtCO$. It should be noted that all stages of CO oxidation on $Pt_{12}Co$ have low activation energies and can proceed at low temperatures. A comparison of the calculated values for the stages of CO oxidation on $Pt_{12}Co$ and Pt_{13} shows how $Pt_{12}Co$ is active. It is noteworthy that the cobalt atom is not in the active center of the cluster, and the oxidation of CO on bimetallic cluster proceeds only on platinum atoms. Cobalt probably changes the electronic properties of the cluster, so that an alternative and more advantageous oxidation mechanism takes place.

Catalytic Properties of Monometallic and Bimetallic Nanopowders Containing Platinum and Cobalt in the Oxidation of CO

The catalytic properties of Pt nanopowder and a disordered solid solution of $Pt_{0.5}Co_{0.5}$ were compared. Figure 5 shows the temperature dependences of the conversion of CO on Pt and $Pt_{0.5}Co_{0.5}$ samples. It is clear that when the temperature was raised, the conversion of CO grew to 100% and remained unchanged, due to the absence of side reactions. It should be noted that oxidation began at 150°C on Pt and full conversion was reached at 194°C, while the oxidation of CO proceeds on $Pt_{0.5}Co_{0.5}$ at a lower temperature (25°C) and full conversion is achieved at 93°C. $Pt_{0.5}Co_{0.5}$ is therefore more active in the oxidation of CO than Pt. The weak activity of monometallic Pt in the oxidation of CO at low temperatures is usually due to dense coating of the Pt surface with adsorbed CO molecules, which prevent the adsorption and activation of oxygen [23–25]. It is assumed that additional low-temperature oxidation route of CO appears for bimetallic Pt–M (M = Cu, Fe, Co, Ni, etc.), which is realized with a significant surface coverage of metals with the adsorbed CO molecules [10–14]; a "geometric" effect is also important [23, 24]. Such a low-temperature route of CO oxidation on $Pt_{12}Co$ confirms this hypothesis. The quantum-chemical calculations performed in this work show that Pt–Co bimetallic systems are more active than monometallic Pt one in the oxidation of CO even if there are weak coatings and free surface.

CONCLUSIONS

Quantum-chemical simulation of the oxidation of CO on Pt_{13} and $Pt_{12}Co$ clusters, including calculations of the clusters' structure, the change in energy during their interaction with O_2 and CO, their activation energy, and the change in energy in the main stages of CO oxidation shows that bimetallic $Pt_{12}Co$ clusters have better catalytic properties than Pt_{13}. An increase in catalytic activity is due not to geometric factors, but to an electronic effect: the electronic properties of a platinum cluster change when cobalt is introduced into its composition. Experimental studies of the oxidation of CO on Pt nanoparticles and bimetallic disordered solid solutions of $Pt_{0.5}Co_{0.5}$ confirmed that the last has higher catalytic characteristics and low-temperature activity.

FUNDING

This work was performed as part of a State Task for the Boreskov Institute of Catalysis, Siberian Branch, Russian Academy of Sciences; project no. AAAA-A17-117041710088-0.

ACKNOWLEDGMENTS

This work was performed on equipment of the High-Performance Computing Resources center of Moscow State University.

REFERENCES

1. R. Hammami, A. Dhouib, S. Fernandez, et al., Catal. Today **139**, 227 (2008).
2. D. Weijing, Z. Weihong, Z. Xiaodong, et al., Energy Proc. **152**, 997 (2018).
3. C. J. H. Jacobsen, S. Dahl, B. S. Clausen, et al., J. Am. Chem. Soc. **123**, 8404 (2001).
4. W. Yu, M. D. Porosoff, and J. G. Chen, Chem. Rev. **112**, 5780 (2012).
5. M. A. van Spronsen, J. W. M. Frenkenb, and I. M. N. Groot, Chem. Soc. Rev. **46**, 4347 (2017).
6. J. Cisternas, P. Holmes, I. G. Kevrekidis, et al., J. Chem. Phys. **118**, 3312 (2003).
7. I. Smiechowicz, I. Kocemba, J. Rogowski, et al., React. Kinet. Mech. Catal. **124**, 633 (2018).
8. R. J. Baxter and P. J. Hu, Chem. Phys. **116**, 4379 (2002).
9. D. Merki and X. Hu, Energy Environ. Sci. **4**, 3878 (2011).

10. T. Komatsu and A. Tamura, J. Catal. **258**, 306 (2008).
11. Q. Fu, W. X. Li, Y. X. Yao, et al., Science (Washington, DC, U. S.) **328**, 1141 (2010).
12. C. Zhang, W. Lv, Q. Yang, et al., Appl. Surf. Sci. **258**, 7795 (2012).
13. R. Mu, Q. Fu, H. Xu, et al., J. Am. Chem. Soc. **133**, 1978 (2011).
14. K. Sato, A. Ito, H. Tomonaga, et al., ChemplusChem (2019, in press). https://doi.org/10.1002/cplu.201800542
15. D. Xu, Z. Liu, H. Yang, et al., Angew. Chem. Int. Ed. **48**, 4217 (2009).
16. J. Singh, R. C. Nelson, B. C. Vicente, et al., Phys. Chem. Chem. Phys. **12**, 5668 (2010).
17. J. P. Perdew, K. Burke, and M. Ernzerhof, Phys. Rev. Lett. **77**, 3865 (1996).
18. W. J. Stevens, M. Krauss, H. Basch, et al., Can. J. Chem. **70**, 612 (1992).
19. H. B. Schlegel, J. Comput. Chem. **3**, 214 (1982).
20. C. Gonzalez and H. B. Schlegel, J. Chem. Phys. **90**, 2154 (1989).
21. D. N. Laikov and Yu. A. Ustynyuk, Russ. Chem. Bull. **54**, 820 (2005).
22. V. Sadovnichy, A. Tikhonravov, Vl. Voevodin, and V. Opanasenko, *Contemporary High Performance Computing: From Petascale toward Exascale* (CRC, Chapman and Hall, CRC Comput. Sci., Boca Raton, FL, 2013), p. 283.
23. D. I. Potemkin, E. Yu. Filatov, A. V. Zadesenets, et al., Catal. Commun. **100**, 232 (2017).
24. D. I. Potemkin, E. S. Saparbaev, A. V. Zadesenets, et al., Catal. Ind. **10**, 62 (2018).
25. D. I. Potemkin, M. V. Konishcheva, A. V. Zadesenets, et al., Kinet. Catal. **59**, 514 (2018).
26. T. Imaoka, H. Kitazawa, W.-J. Chun, et al., J. Am. Chem. Soc. **135**, 13089 (2013).
27. N. Watari and S. Ohnishi, Phys. Rev. B **58**, 1665 (1998).
28. J. Sun, X. Xie, B. Cao, et al., Comput. Theor. Chem. **1107**, 127 (2017).
29. V. Kumar and Y. Kawazoe, Phys. Rev. B **77**, 205418 (2008).
30. Y. Sun, M. Zhang, and R. Fournier, Phys. Rev. B **77**, 075435 (2008).
31. M. Zhang and R. Fournier, Phys. Rev. A **79**, 043203 (2009).
32. P. L. Rodríguez-Kessler and A. R. Rodríguez-Domínguez, J. Chem. Phys. **143**, 184312 (2015).
33. O. C. Compton and F. E. Osterloh, J. Am. Chem. Soc. **129**, 7793 (2007).
34. R. Wallace, C.R. Chim. **14**, 1117 (2011).
35. F. Aguilera-Granja, R. C. Longo, L. J. Gallego, et al., J. Chem. Phys. **132**, 184507 (2010).

Translated by A. Tulyabaev